UC San Diego
UC San Diego Previously Published Works

Title
Programmable Screen for Patterning Magnetic Fields

Permalink
https://escholarship.org/uc/item/2qs9083m

Journal
IEEE Transactions on Microwave Theory and Techniques, 62(3)

ISSN
0018-9480

Authors
Gao, Fei
Zhang, Fushun
Huang, Ming
et al.

Publication Date
2014-03-01

DOI
10.1109/tmtt.2014.2299763

Peer reviewed

Programmable Screen for Patterning Magnetic Fields

Fei Gao, *Student Member, IEEE*, Fushun Zhang, Ming Huang, *Student Member, IEEE*, and Daniel F. Sievenpiper, *Fellow, IEEE*

Abstract—We present the design and experimental demonstration of a magnetic screen, which can pattern magnetic field into 256 programmable spots of small sub-wavelength dimension. A design methodology is outlined for designing a near-field plate to achieve a desired focus, and its implementation is discussed. Simulation using a full-wave electromagnetic solver clearly demonstrates focused magnetic field spots and that the presented structure has a stronger magnetic field compared with a conventional coil at the same focusing distance. A sample of thickness 2.1 mm with 16 layers, in which there are 32 unclosed loops for focusing on each of the eight layers and optimized guiding strips on the other eight layers, is fabricated and measured. The measurement results agree well with the simulation results. Finally, the response of the magnetic screen in the time domain is measured and computed showing the screen can be operated under pulse excitation. Such a device, capable of producing a programmable focused magnetic field, will find applications in biomedical devices, near-field imaging systems, data storage, and electromechanical actuators.

Index Terms—Focusing, magnetic screen, near field, pattern, time domain, transcranial magnetic stimulation (TMS).

I. INTRODUCTION

ELECTROMAGNETIC near-field research has received considerable attention since Synge showed that detecting the near field of an object equals to tapping into the object's sub-wavelength details, which can obtain resolution beyond the diffraction limit [1]. Experimental verification showing that near-field imaging is possible was reported in [2]–[4]. In addition to the image processing, sub-wavelength focusing of the electromagnetic field as a key technique in both optical and microwave regimes has intrigued scientists and engineers alike. Many papers discussing near-field focusing are published that include superlens [5], aperiodic gold nanowire arrays [6], sub-wavelength spaced slot arrays [7], and dielectric gratings [8]. A near-field plate based on radiationless interference was recently designed and implemented in the microwave domain [9]–[12], where the radiationless field by the source was redistributed on the near-field plate as a second source to make the final field generate a sub-wavelength focal spot some distance away. The near-field plate was designed and experimentally demonstrated in the microwave domain [10]–[13]. The near-field focusing based on this method was also investigated in the optical regime [14]–[16]. In addition to focusing the electrical field, focusing the magnetic field has intrigued many scientists [17]–[19]. Although some near-field plates can focus the magnetic fields from a plane wave or that produced by a dipole or a monopole to spots or lines, they are not designed to focus the magnetic fields perpendicular to it [20], [21]. An investigation pertaining to the manipulation of kilohertz-band magnetic fields in air was first reported in [17] and experimental demonstration was presented in [18], where a focused magnetic field strip is produced.

In the field of neuroscience, an important goal is to modulate activity in the body [22]. The electroencephalogram (EEG) and functional magnetic resonance imaging (fMRI) provide good ways to read signals from the brain, and efforts are underway to improve their resolution [23]. However, we are still lacking precise ways to write signals to the brain. Biomedical applications such as transcranial magnetic stimulation (TMS) produce intense pulsed magnetic fields into a circular shaped spot to make therapeutic effects in the brain [24]. This technique is used to treat neurological disorders such as depression. However, presently TMS using a pair of coils, with poor focusing performance, stimulate a region of the brain roughly the size of a golf ball. Seeking an effective way to precisely focus magnetic field inside the body is a big challenge to existing biomedical devices.

In this paper, we present a new type of digital field manipulation screen that gives a possible solution that may enable us to program the field profile and therefore current profile inside tissues for new approaches to biological applications of electromagnetics. The presented structure can focus a magnetic field into spot rather than strip in the focal plane. Using the proposed structure would allow for finer resolution and electronic scanning to rapidly stimulate various areas of the tissue. Compared to the conventional coil, this structure increases the resolution of the magnetic field focusing, as well as the field intensity within the nondiffractive range.

This paper is organized as follows. In Section II, a general design procedure to generate a desired focusing pattern is discussed. The near-field plate is examined through full-wave simulations as a more effective and practical method for gen-
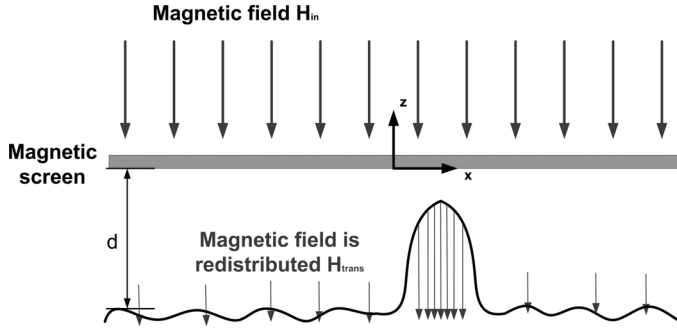
Fig. 1. Magnetic screen ($z = 0$) and focal plane ($z = d$). Incident magnetic field passes through the magnetic screen where induced current would be produced. The interference between the induced filed and original field can focus magnetic pattern we want.

erating a programmable magnetic field pattern. In Section III, the design procedure for such a magnetic screen is reviewed. The operation and design is also verified through full-wave simulation. A sample with the ability to produce 256 programmable focused magnetic field spots is fabricated and measured. The depth of focusing is measured. All of the simulations in this paper are implemented by using Ansoft HFSS 15.0, a finite-element-method-based high-frequency structure simulation package.

II. UNIT CELL

A. Basic Principle for Designing a Near-Field Plate

A general procedure for designing a near-field plate was discussed in [13] where incident waves were assumed to be parallel to the near-field focusing plate, and the plates were designed by surface impedances computed by taking the ratio of the field at the plate's surface to the derived current density. The procedure in [13] can enable one to design a plate that can achieve a focused electromagnetic radiation pattern along a focal plane in the plate's reactive near-field region. The magnetic field focusing is outlined in [17]. Compared with the focusing of the electric field, the curl of the induced current density at the plate is shown to be an important design parameter in the magnetic field focusing. Focusing plates like a pair of metallic periodic-ladder structures [17] and a single defected loop array structure [19] were analyzed in detail based on the current distribution. Here, a design flow for designing a near-field focusing plate in the magnetic field is also presented. The design of the plate is dependent on both the source excitation, as well as the desired focus. A model of focusing plate concept is shown in Fig. 1, which is composed of a focusing plate we call the magnetic screen located along at $z = 0$, and the focal plane is at $z = -d$. When the magnetic field illuminates the focusing plate from the positive z axis, the focused magnetic field pattern is formed on the focal plane.

For the sake of simplicity, lossless conductive strips are assumed. The incident magnetic field along the negative z-direction is applied from the backside of the near-field focusing plate, where curl current is induced in the strips to create a magnetic

field in the opposite direction of the incident field. Thus, the design procedure starts by formulating the wave (1) where the curl of the induced current density is located on the right-hand side of the equation,

$$-(\nabla^2 + k_0^2)\vec{H} = \nabla \times \vec{J} \tag{1}$$

in which $\vec{H}$ is the incident magnetic field, $\vec{J}$ is the induced current density, and k_0 is the wavenumber in free space. The magnetic field can then be computed by integrating the 2-D Green's function multiplied by the curl of the induced current density

$$\vec{H}(x, y, z) = \iint G(x, y, z, x', y', z' = 0)\nabla$$
$$\times \vec{J}(x', y')dx'dy'. \tag{2}$$

The field at $z = 0$ satisfies the following equation:

$$\vec{H}_{\text{trans}}(x, y, z = 0)$$
$$= \vec{H}_{in}(x, y, z = 0)$$
$$- \frac{1}{4\pi} \iint G(x, y, z = 0, x', y', z' = 0)\nabla$$
$$\times \vec{J}(x', y')dx'dy'. \tag{3}$$

From the theory of back-propagating in [14], once a desired magnetic field distribution $H_{\text{trans}}(x, y, z = -d)$ is set, $H_{\text{trans}}(x, y, z = 0)$ should be calculated using the following steps.

First, a Fourier transform is taken on the focal plane to get its plane-wave spectrum $\vec{H}_{\text{trans}}(k_x, k_y, z = -d)$, where the harmonic time dependence is e^{jwt}

$$\vec{H}_{\text{trans}}(k_x, k_y, z = -d)$$
$$= \int_{-\infty}^{\infty} \int_{-\infty}^{\infty} \vec{H}_{\text{trans}}(x'', y'', z = -d)e^{+j(k_{x''}x'' + k_{y''}y'')}dx''dy''. \tag{4}$$

Then make the transformation using the back-propagation method,

$$\vec{H}_{\text{trans}}(k_x, k_y, z = 0) = \vec{H}_{\text{trans}}(k_x, k_y, -d)e^{+j(k_x x + k_y y - k_z d)} \tag{5}$$

where

$$k_z = \sqrt{k_0^2 - k_x^2 - k_y^2}, \qquad \text{when } k_x^2 + k_y^2 < k_0^2$$
$$k_z = -j\sqrt{k_0^2 - k_x^2 - k_y^2}, \qquad \text{when } k_x^2 + k_y^2 > k_0^2. \tag{6}$$

Substituting $H_{\text{trans}}(x, y, z = 0)$ into (3), we can get the field distribution needed under the specified incident magnetic field.

In the study of electric field focusing [13], the surface impedance needs to be imaginary in the design of a passive device. While in the focusing of magnetic field, the curl of induced current is an important parameter in the process of design. If we define the ratio of the magnetic field to the curl of the induced current density as a counterpart parameter, it

This article has been accepted for inclusion in a future issue of this journal. Content is final as presented, with the exception of pagination.

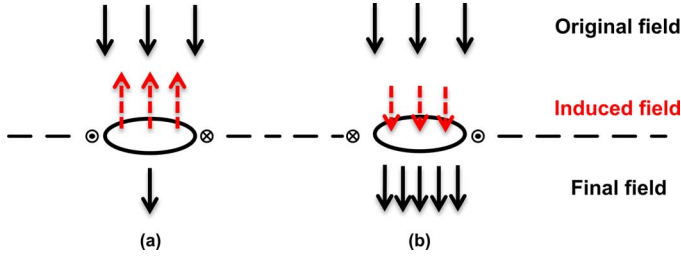GAO *et al.*: PROGRAMMABLE SCREEN FOR PATTERNING MAGNETIC FIELDS

3

Fig. 2. Functions of magnetic screen are to: (a) cancel the original field in the suppressed area and (b) focus the field in the needed area.
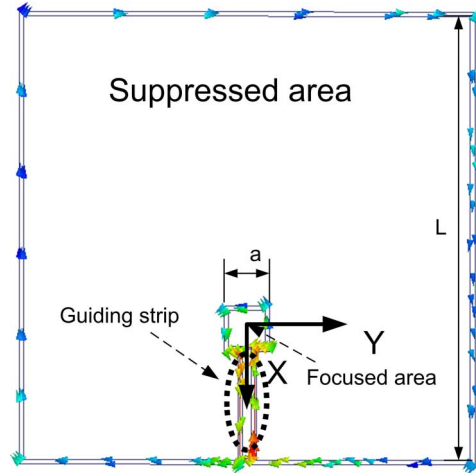

Fig. 3. Unit of the magnetic screen. The focused area is at the origin of coordinate. The current encircling the suppressed is clockwise and that encircling the focused area is counter-clockwise.

Fig. 4. Normalized amplitude of simulated magnetic field of a unit cell at $z = -0.5$ mm. The inset is the simulated 2-D magnetic field.

may have the real part. This could be explained by the equation for induced current. For electric field, the right-hand side of (1) is $-j\omega\mu\vec{J}$, where ω and μ are the angular frequency and permeability. Here, we use induced current density in the focusing plate as the design parameter to explain how to obtain the desired magnetic field pattern.

B. Unit Cell Design

Observing induced current in the structure presented by [17]–[19], we will find the closed structure can excite a magnetic field that is opposite in direction to that of the incident magnetic field. Thus, a closed structure can be used for collecting the near magnetic field energy in order to suppress the field in the focal plane. The collected energy can then be controlled to produce a magnetic field in the position we want, namely, focusing. Thus, the near-field plate must have two functions shown in Fig. 2. For the suppressed area, the induced field by a magnetic screen is in the opposite direction as the original field. For the focused area, the magnetic screen is invisible to the original field. The configuration of the unit cell and induced current illuminated by a magnetic field from the positive z direction is shown in Fig. 3. It consists of a large square loop and a small unclosed loop connected by a pair of strips. The induced current is clockwise on the bigger loop and counter-clockwise on the small loop.
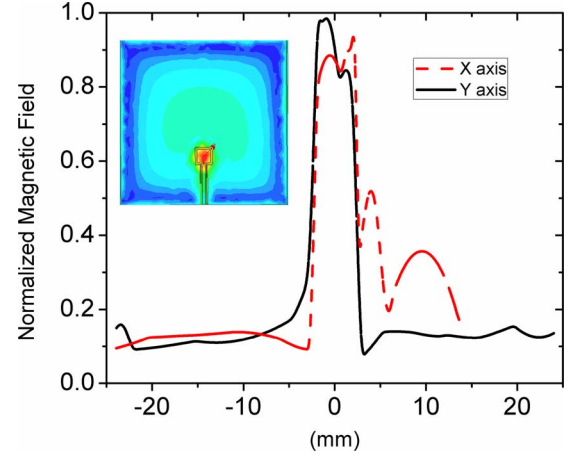
The z-component of scattered magnetic field by the structure in Fig. 3 can be computed using (2), which was given by

$$
\begin{aligned}
\vec{H}(x, y, z) &= \iint G(x, y, z, x', y', z' = 0)\nabla \times \vec{J}(x', y')dx'dy' \\
&= \iint G(x, y, z, x', y', z' = 0) \\
&\quad \times \left(\frac{\partial J_y}{\partial x} - \frac{\partial J_x}{\partial y}\right) dx'dy' \\
&= \frac{1}{4}\pi \iint \frac{1}{\left[(x-x')^2 + (y-y')^2 + z^2\right]^{1/2}} \\
&\quad \times \left(\frac{\partial J_y}{\partial x} - \frac{\partial J_x}{\partial y}\right) dx'dy'.
\end{aligned}
\tag{7}
$$

If the structure in Fig. 3 has a high aspect ratio, (7) would be a 1-D problem like [17] and [19] that can be simplified using Hankel function. The normalized magnetic field norm $\|H\|$ was simulated under an incident field created by the coil 15 mm above at 1 MHz with $L = 50$ mm and $a = 5$ mm. Observe that the clockwise current induced on the outer loop creates a magnetic field, $\nabla^2\vec{H}^2 = -\nabla \times \vec{J}$, that is opposite in direction to that of the incident magnetic field. In the area between the two loops, the magnetic field is suppressed, while it is focused passing through the small loop. The simulated focusing results are shown in Fig. 4, where the abscissa runs from -24 mm to 24 mm along two cut lines in the x- and y-direction, respectively, positioned at the center of the focused area at $z = -1$ mm.

C. Programmable

In the previous section, the magnetic field focusing has been achievable. However, the focusing field at different positions at the same time or controlling the focused field pattern is still a problem. Making the structure programmable means the structure presented by Fig. 3 must have more than one focusing area

This article has been accepted for inclusion in a future issue of this journal. Content is final as presented, with the exception of pagination.

4

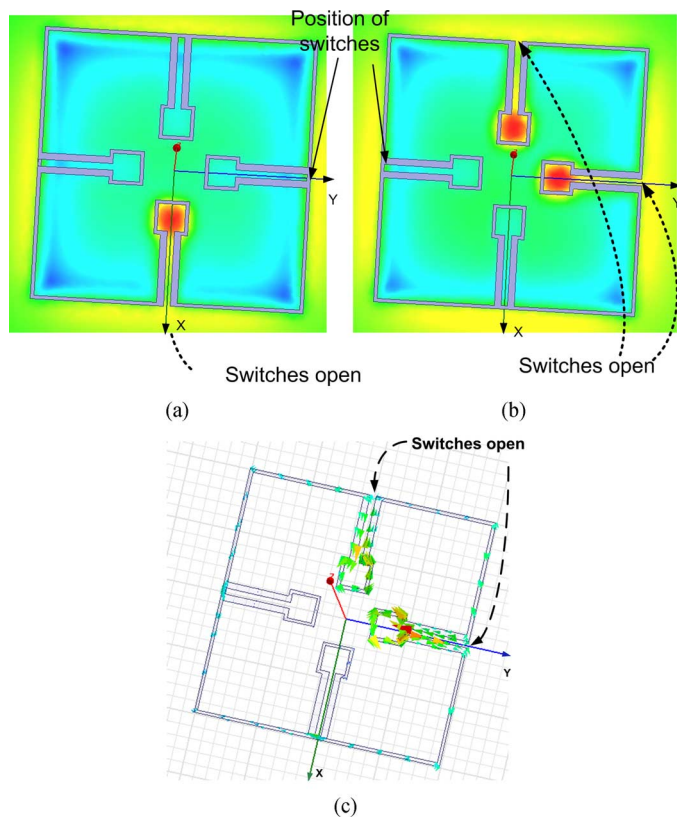IEEE TRANSACTIONS ON MICROWAVE THEORY AND TECHNIQUES

Fig. 5. Programmable focusing design of unit cell. (a) Simulated 2-D magnetic field with one switch open. (b) Simulated 2-D magnetic field with two switches open. (c) Induced current on the structure with two switches open.
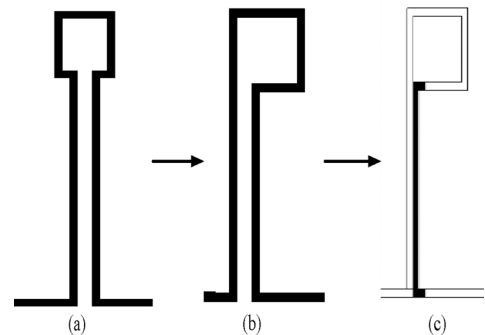

Fig. 6. Evolution of the guiding strip. (a) Pair of guiding strips in the same plane is positioned in the center of the focused area. (b) Pair of guiding strips in the same plane is moved to the edge of the focusing region. (c) One of the guiding strips is shifted up to another plane.
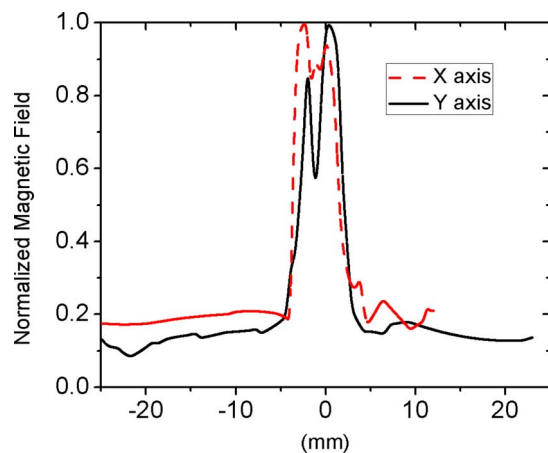

Fig. 7. Normalized amplitude of simulated magnetic field of a unit structure with the improved guiding strip at $z = -0.5$ mm.

with the field suppressed in other areas, and switches to determine which areas are active. In Fig. 5 is the presented programmable near-field plate that has the ability to focus the magnetic field to four different spots. The switches are located at the junctions between the guiding strip and outer loop. The switch is on when the current can pass through the smaller loop encircling the focused area, otherwise the switch is off. Thus, the magnetic field can be focused at different positions by opening the appropriate switches.

The 2-D magnetic field plot at $z = -0.05$ mm is shown in Fig. 5(a) and the induced current in Fig. 5(b). For the case of focusing in two spots, little induced current can been seen on the smaller loops and guiding strips, which are off. This means the switch can successfully control the focusing area without destroying the suppressed part. Thus, we can focus at more than one spot at a time.

D. Improvement of the Guiding Strip

From the focusing performance shown by Fig. 4, the suppressed field in the x-direction is not ideal due to existence of the guiding strip in Fig. 3. The magnetic field produced by the guiding strip is in the same direction with the incident magnetic field; and inevitably passes through the near-field plate and deteriorates the magnetic field pattern. If the current on the guiding strip decreases, the magnetic field created by it would be weak as well as the focusing efficiency because the process of collecting the original field is interrupted. Since the focusing performance is valued on the focal plane, the magnetic field produced by the

guiding strip can be redirected to another position far away from the focal plane. Fig. 6 gives the evolution of the guiding strip for removing the effect on the focusing performance. The guiding strips in Fig. 6(b) are just moved to the edge of the focused coil. It has the same performance as the original unit, but this change is necessary for the array design. In Fig. 6(c), two guiding strips are located on different layers along the z-direction.

The performance of the focused magnetic field with improved guiding strip is shown in Fig. 7. Compared with the results in Fig. 4, the field near the peak in the x-direction is suppressed very well without the grating beam. The only drawback for this kind of guiding strip is to make the unit more complicated. We can see later using this structure as the unit cell requires that the magnetic screen has double layers.

E. Frequency Response

The bandwidth of the signals for TMS systems spans from dc to the kilohertz or megahertz range since they usually operate in pulsed current mode [22]. However, most published focusing techniques are just studied at one frequency point [10], [18], [19], [25]. Actually, assuming the incident magnetic field is ideal; the curl of the induced magnetic field is the only design parameter for a set magnetic field pattern. Considering the structure we presented is not a resonant one, we have reason to conclude that the structure can cover a very wide operating
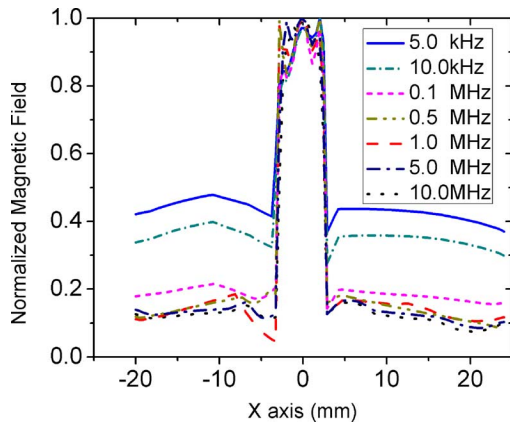
This article has been accepted for inclusion in a future issue of this journal. Content is final as presented, with the exception of pagination.

GAO *et al.*: PROGRAMMABLE SCREEN FOR PATTERNING MAGNETIC FIELDS

5

Fig. 8. Normalized amplitude of simulated magnetic field distribution of a unit cell at various frequency points along the X axis at $z = -0.5$ mm.

frequency band with the magnetic field pattern we want. The structure in Fig. 3 with the guiding strip in Fig. 6(c) is simulated at seven sampled points from 5 kHz to 10 MHz. The simulated results are shown in Fig. 8. We can see from the plot that the structure works over a very large frequency band. However, the contrast in the lower frequency range is not as good as at the higher frequencies. From (1), k_0 decreases along with the decrease of the frequency. Thus, for a specified structure, the amplitude of induced current would be smaller for lower frequencies, as well as the induced magnetic field intensity. More fields passing through the suppressed area thus reduce the field contrast. On the other hand, the collected near-field energy is lowered due to the weakness of the induced current. This also makes the focused magnetic field lower. Higher in the suppressed part and lower in the focused area of the magnetic field make the contrast not sharp in the low-frequency points as in the high-frequency points.

There is a notch in the focused area in some frequency points due to phase errors. The notch would be removed if the probed height is moved 0.5 mm up or down.

F. Focused Magnetic Field Intensity

The normalized amplitude of the simulated magnetic field focused by the magnetic screen at various distances from the unit cell is compared with that created by a coil used in the standard TMS technique. The probed magnetic field is along the z-direction positioned at the center of a focused area. From the simulated results in Fig. 9(a), a magnetic field with half maximum value is deeper when increasing the radius of the coil, which means enlarging the size of the coil can be of help to get a deeper magnetic field. In addition, the magnetic field passing through the near-field plate is stronger than that created by the coil of the same size at the same depth. This is because the magnetic field passing through the magnetic screen is created by a much bigger coil. Since enlarging the coil can produce a deeper magnetic field, the focused magnetic field using a larger coil as the source also gets the same effect. When passing through the magnetic screen, the field in some areas is suppressed and transformed into the induced current, which is of assistance for increasing magnetic field intensity in the focusing part. Considering the two points mentioned above, the magnetic screen can

be used to produce deeper magnetic field without sacrificing the focusing resolution. Unfortunately, the contrast between the focused magnetic field and the suppressed one deteriorates along with the increase of focusing distance from the magnetic screen, as shown in Fig. 9(b). However, the focused magnetic field still remains very high compared with that produced by the conventional coil before the contrast disappears. This is very helpful in some situations where a stronger magnetic field is needed, such as for high-resolution TMS. If conventional coils are reduced to improve the resolution, the magnetic field dies off quickly. Thus, it is difficult to produce a strong field with high resolution using conventional coils.

The effect of the size of a large coil as the magnetic field source on the contrast and the focused magnetic field intensity is shown in Fig. 10 where the unit size is $L = 40$ mm and $a = 5$ mm in Fig. 3. The magnetic field is probed in the y-direction 1 mm under the magnetic screen. The contrast is better with the larger source because the magnetic field in the center of the larger coil is more ideal. The direction of the magnetic field passing through the magnetic screen is more congruent and perpendicular to the magnetic screen with a larger source. The contrast would be unchanged when the radius of the source is more than 50 mm in this case. If the source is smaller than the magnetic screen, the field cannot be collected very well due to the magnetic field being far from ideal. Thus the contrast is deteriorated as is indicated when $r = 10$ mm. Fig. 11(b) gives the variation of the absolute focused magnetic field value with the size of the source. From Ampère's circuital law $\nabla \times \vec{H} = \vec{J}$, the farther from the current, the weaker the magnetic field. Thus, the focused magnetic field intensity is decreased when the radius of the source is larger than 50 mm. However, the focused magnetic field intensity is even worse due to the poor focusing performance with very small source. When the input power is doubled, the focused magnetic field intensity is increased by a factor of more than $\sqrt{2}$ when the radius of the large coil is in the range from 40 to 60 mm because the magnetic screen collects the field and focuses it. Considering the contrast and focused magnetic field intensity, the magnetic source should cover the whole magnetic screen or be slightly larger than it.

III. MAGNETIC SCREEN

A. Configuration

Based on the unit cell structure studied above, a magnetic screen with the ability of focusing 256 programmable spots at different positions was designed and manufactured using a printed circuit board (PCB) technique. Fig. 11(a) shows the simulation model on which the switches are indicated. The whole structure was constructed in a spiral form connected with metal vias in order that induced current on each layer is in the same direction. The unit cells have a separation of 0.3 mm where the guiding strip has a space of 0.13 mm between layers. As discussed in the previous section, the optimized structure requires 16 layers rather than eight layers so that the guiding strips overlap. Fig. 11(b) indicates the configuration of the switches to control the focusing positions. The switches in the plot are at the closed state. If one of the strips representing the switches is opened, the area it controls will focus the field underneath. The
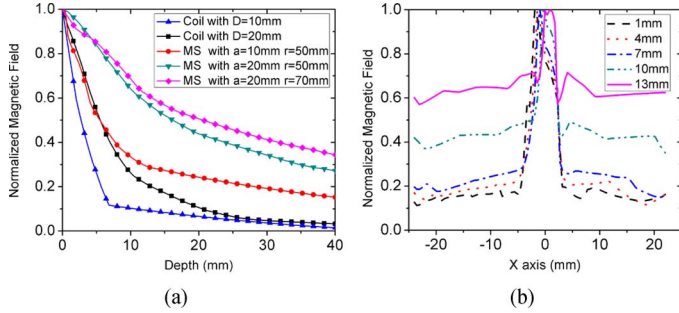
This article has been accepted for inclusion in a future issue of this journal. Content is final as presented, with the exception of pagination.

6

IEEE TRANSACTIONS ON MICROWAVE THEORY AND TECHNIQUES

Fig. 9. (a) Normalized amplitude of simulated magnetic field along the z-direction sampled at the center of the focused area. D is the diameter of the conventional coil. MS represents the magnetic screen. r is the radius of the larger coil above the magnetic screen, which is used as magnetic field source in the simulation. (b) Normalized amplitude of simulated magnetic field along the x axis at various distances from the unit cell.
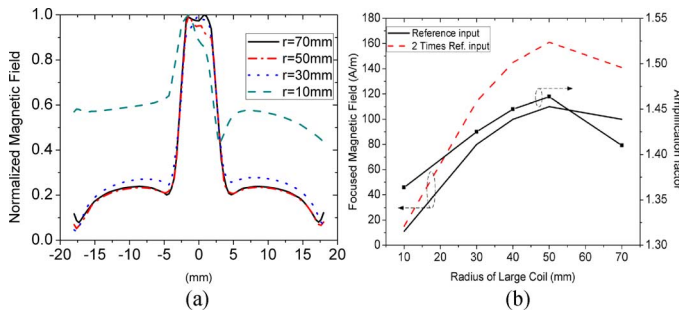

Fig. 10. Effect of the magnetic source on the contrast and the focused magnetic field intensity. (a) Variation of the contrast with the radius of the large coil. (b) Variation of the maximum focused magnetic field intensity along with the radius of the large coil.

sample has a thickness of 2.1 mm, shown in Fig. 11(c), with the FR4 as the support material. All of the switches are located on the top layer in order to facilitate the measurement.

The complicated employment of switches deteriorates the focusing performance, as shown in Fig. 12. The contrast is worse. If higher quality focusing performance is needed, alternative arrangement of switches can be used, such as placing them internal to the layers, or directly at each of the small loops. In our experiment, we use this switch configuration to simplify the fabrication and measurement.

B. Experimental Results

The performance of the magnetic screen is verified in the frequency domain and time domain. The measurement system is illustrated in Fig. 13. The upper three pieces of equipment are for frequency-domain measurements. The green large coil (in the online version) having a diameter of 300 mm, slightly larger than the sample, is the magnetic source excited by the signal generator (see the inset of Fig. 13). A small loop with a diameter of 4 mm is used as a magnetic field probe, and scans the near field using an automatically controlled 3-D translation stage. The signal received by the small loop is analyzed by the signal analyzer. The translation stage and the signal analyzer are controlled by NI LabVIEW software, which is also responsible for near-field scanner and data acquisition. The near field was measured over an area 180 mm × 180 mm with a step of 1.75 mm at different distances from the magnetic screen.
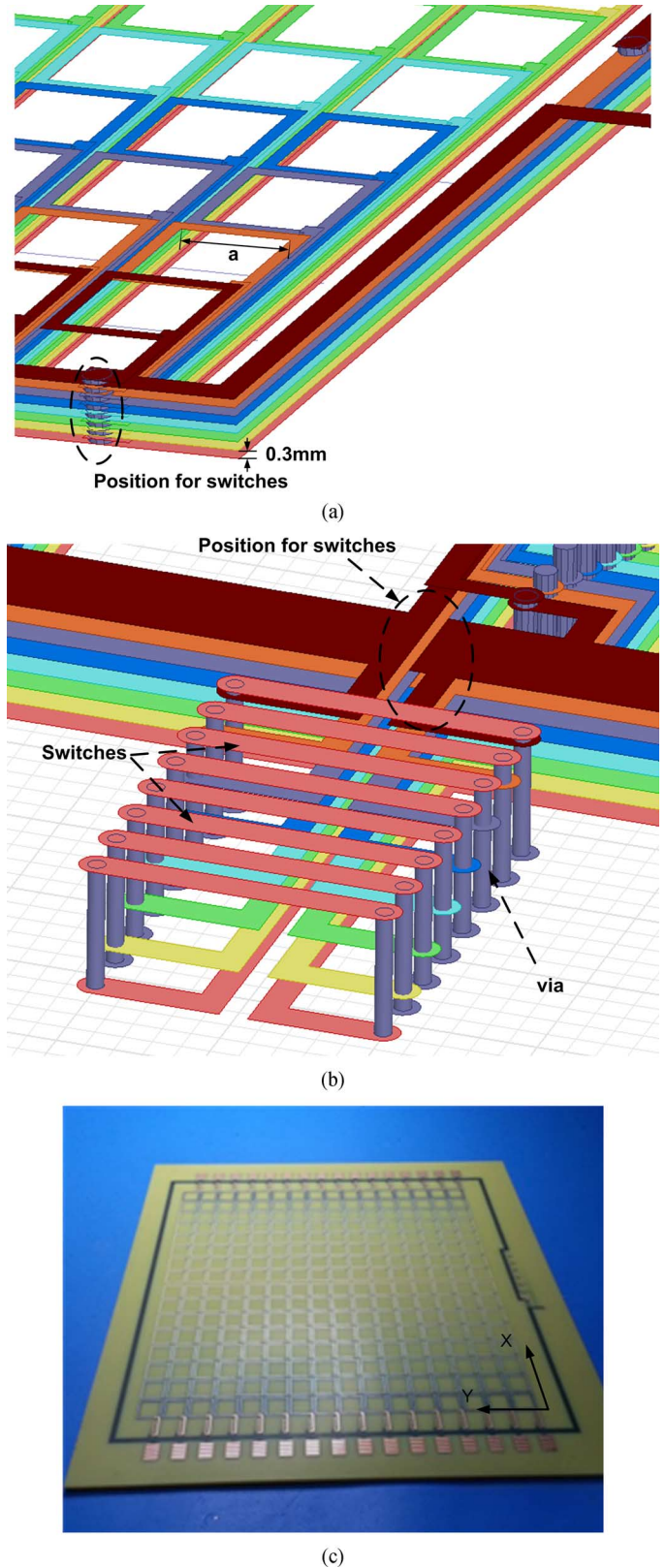

Fig. 11. (a) Simulation model of a magnetic screen with 16 layers in which focusing areas are included on eight layers spaced by 0.3 mm. (b) Configuration of switches used in the measurement. (c) Fabricated magnetic screen. (Dimension: $a = 10$ mm).

The magnetic field along the xy plane and a complete 2-D scan at 1 mm above the magnetic screen are given in Fig. 14. Fig. 14(a) is a 2-D field plot for the whole structure at

This article has been accepted for inclusion in a future issue of this journal. Content is final as presented, with the exception of pagination.

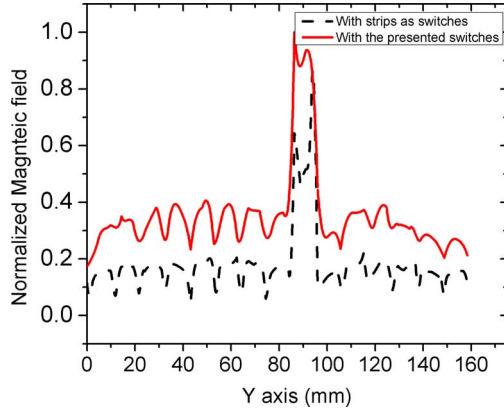GAO *et al.*: PROGRAMMABLE SCREEN FOR PATTERNING MAGNETIC FIELDS

7

Fig. 12. Comparison of the effects on the performance of focusing with and without the presented switches.
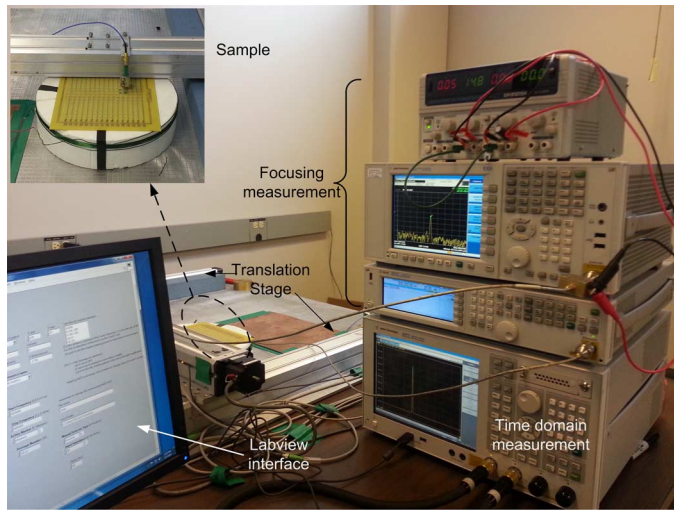

Fig. 13. Measurement setup for frequency response. Computer is used to control the track and signal analyzer. The inset shows the sample and bigger coil as the magnetic field source.
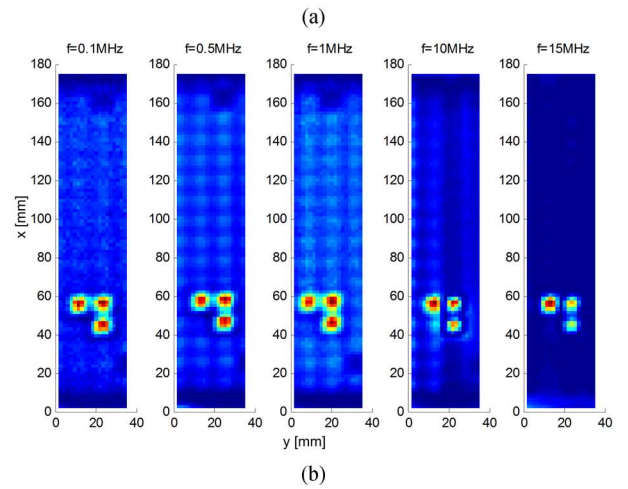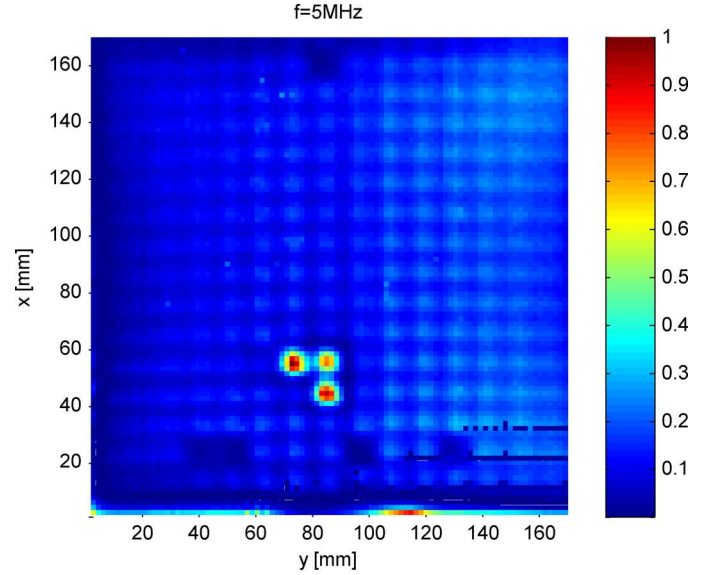

Fig. 14. Normalized amplitude of measured magnetic field energy for the sample [coordinate shown in Fig. 11(c)]. (a) 2-D measured magnetic field energy plot at $f = 5$ MHz. (b) Snapshots of measured magnetic field energy plot for focused area at $f = 0.1$ MHz, 0.5 MHz, 1 MHz, 10 MHz and 15 MHz.

5 MHz. The snapshots for other frequency points are shown in Fig. 14(b). These 2-D field distributions clearly demonstrate the focused magnetic field that is intended.

The field slices in the focusing area along the x-direction are shown in Fig. 15 in which the magnetic field is normalized to the maximum value in the whole focal plane at each frequency point. Compared with the magnetic field produced by the large coil, the field passing through the magnetic screen is redistributed and that in the focused area is increased as shown in Fig. 15(a) due to energy transformation from the large magnetic flux that passes through the area between the large loop and the small one. The measured magnetic field versus frequency is shown in Fig. 15(b) and (c). Focusing contrast is better at higher frequencies due to the strong induced current on the structure. This phenomenon agrees well with the simulated results. The measured focusing contrast at 1 MHz is little worse than the simulated one in Fig. 12. The difference between the simulated and measured contrast can be explained by several factors. It is not unexpected to see some difference between simulation and measurement due to the details of the feed for the magnetic

source. Also, automatic positioner and other details of the environment can affect the magnetic field distribution. Errors in the measurement equipment and small discrepancies in manufacture are also expected. The probe positions where the peak of the focused magnetic field is averaged or cannot be probed well will also have an effect on the contrast.

Fig. 16 provides the normalized amplitude of measured magnetic field along the same x axis at several distances away from the magnetic screen. The magnetic field is normalized to the peak value at each slice for the comparison of the contrast. The contrast deteriorates with the increase in distance. The non-diffractive range is 18 mm at 1 MHz and 20 mm at 15 MHz. The contrast at 15 MHz does not change significantly compared with that at 1 MHz. In addition, Fig. 17 provides the normalized magnetic field intensity along the z axis. The measured data was obtained using the magnetic source with $r = 150$ mm. The distance at the same attenuation rate point as shown in Fig. 18 is slightly larger than the simulated results using the magnetic
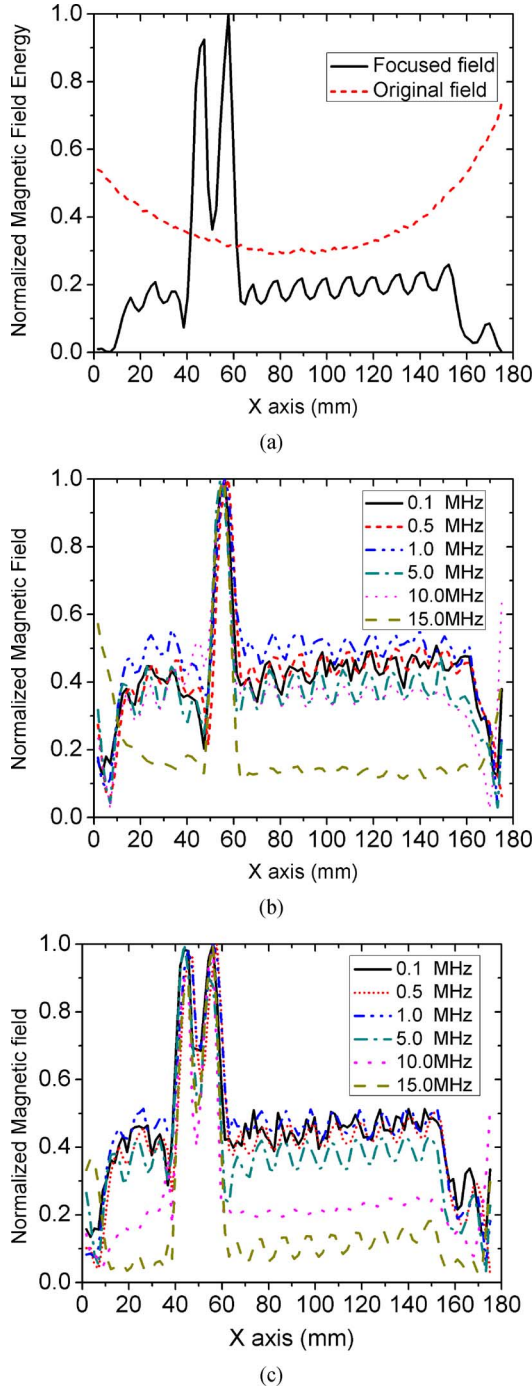
This article has been accepted for inclusion in a future issue of this journal. Content is final as presented, with the exception of pagination.

8   IEEE TRANSACTIONS ON MICROWAVE THEORY AND TECHNIQUES

(a)

(b)

(c)

Fig. 15. Normalized magnetic field magnitude 1 mm away from the magnetic screen along the X axis [shown in Fig. 11(c)]. (a) Comparison of measured magnetic field energy with and without magnetic screen along the X axis cut through one focused area [shown in Fig. 14(b)]. (b) Normalized amplitude of measured magnetic field at different frequency points along x axis cut through one focused area [shown in Fig. 14(a) and (b)]. (c) Normalized amplitude of measured magnetic field at different frequency points along x axis cut through two focused areas [shown in Fig. 14(a) and (b)].

(a)

(b)

Fig. 16. Normalized amplitude of measured magnetic field under the focused area along the x-direction at various distances away the magnetic screen. (a) 1 MHz. (b) 15 MHz.
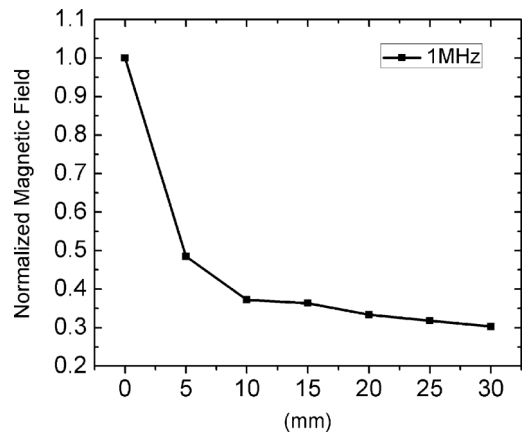
Fig. 17. Normalized amplitude of measured magnetic field under the focused area along z-direction at 1 MHz.

source with $r = 50$ mm. This is because of the loss from using FR4 as the support material.

In the application of TMS, the source is in the form of a current pulse. Thus, it is necessary to get the response of the magnetic screen in the time domain. In our measurement, a vector network analyzer (VNA) E3071C (shown in Fig. 13) is used
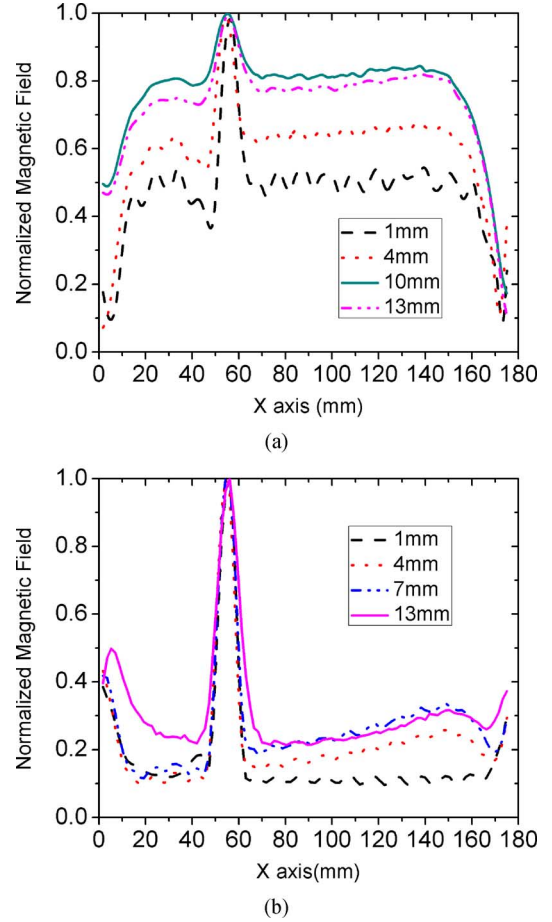
to get the response in the time domain. First, the frequency response S_{21} can be obtained with the magnetic screen and S'_{21} without the magnetic screen. Considering that there are no non-linear components in the magnetic screen, we deal with the magnetic screen as a linear time invariant device. The frequency response of the magnetic screen can be computed using the following equation:

This article has been accepted for inclusion in a future issue of this journal. Content is final as presented, with the exception of pagination.

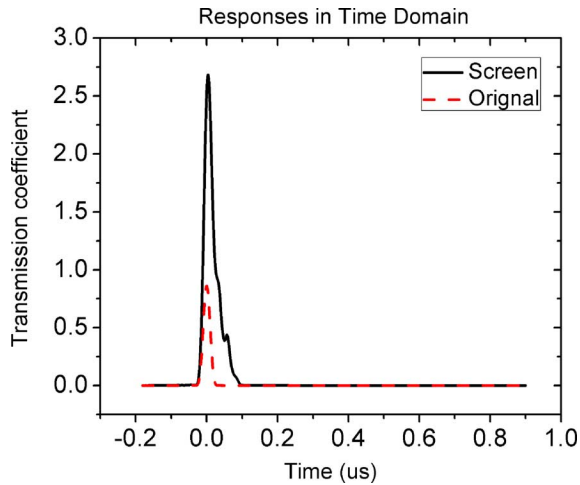GAO *et al.*: PROGRAMMABLE SCREEN FOR PATTERNING MAGNETIC FIELDS 9

Fig. 18. Response of magnetic screen using the transformer algorithm. The solid line is the response with two ports of VNA connected directly. The dotted line is the response of magnetic screen.

$$H_{ms} = \frac{S_{21}}{S'_{21}}. \tag{8}$$

Once the frequency response of the magnetic screen is obtained, its response in the time domain can be computed using an inverse of fast Fourier transformation (IFFT) method. In our measurement, 1044 frequency points are captured spanning from 300 kHz–100 MHz. The IFFT is based on the embedded algorithm in the vector network [26]. The response of the magnetic screen in the time domain is illustrated in Fig. 18. The original signal is the transmission coefficient when connecting two ports of the VNA directly. The screen signal is the transmission coefficient of the magnetic screen obtained by using the method discussed above. The transmission coefficient for the magnetic screen is much higher than unity, which is expected due to the focusing ability of the magnetic screen. In addition, the peak of the magnetic screen has a small delay compared with that of the original signal due to the thickness of the magnetic screen. Some ringing effect is seen on the trailing edge, which is from the phase difference of the signal, and probe position error with and without the magnetic screen.

IV. CONCLUSION

A magnetic field focusing technique has been discussed in this paper, and a programmable magnetic screen has been presented that has the ability to focus a broad area magnetic field into a 10-mm square area. A measurement setup for determining the response of the magnetic screen in the frequency domain and time domain has been provided. Experimental results have clearly demonstrated the focused magnetic field. Compared to the conventional coil applied in TMS, the presented structure can provide the magnetic focusing within a nondiffractive range. An improved switch arrangement may be necessary to increase the contrast between the focused fields and the suppressed region in the future. The new device may enable us to program the field profile, and therefore, the current profile inside tissues for new approaches to biological

applications of electromagnetics. Also, the ability to focus the field at different positions at the same time can generate new capabilities with important applications such as providing sensory feedback to the brain for systems that are currently under development such as direct brain control of vehicles, aircraft, or prosthetic systems, or for more realistic combat simulators for training. In addition, the magnetic field focusing technique can be used to enhance the magnetic force in electromechanical actuators and transducers.

REFERENCES

[1] E. H. Synge, "A suggested method for extending the microscopic resolution into the ultramicroscopic region," *Phil. Mag.*, vol. 6, pp. 356–362, 1928.
[2] D. W. Pohl, W. Denk, and M. Lanz, "Optical stethoscopy: Image recording with resolution $\lambda/20$," *Appl. Phys. Lett.*, vol. 44, pp. 651–653, Apr. 1984.
[3] A. Lewis, M. Isaacson, A. Harootunian, and A. Murray, "Development of a 500-Å spatial-resolution light-microscope," *Ultramicroscopy*, vol. 13, pp. 227–231, 1984.
[4] E. A. Ash and G. Nicholls, "Super-resolution aperture scanning microscope," *Nature*, vol. 237, pp. 510–512, Jun. 1972.
[5] J. B. Pendry, "Negative refraction makes a perfect lens," *Phys. Rev. Lett.*, vol. 85, no. 18, pp. 3966–3969, Oct. 2000.
[6] L. Verslegers, P. B. Catrysse, Z. Yu, and S. Fan, "Deep-subwavelength focusing and steering of light in an aperiodic metallic waveguide array," *Phys. Rev. Lett.*, vol. 103, Jul. 2009, Art. ID 033902.
[7] L. Markley, A. M. H. Wong, Y. Wang, and G. V. Eleftheriades, "Spatially shifted beam approach to subwavelength focusing," *Phys. Rev. Lett.*, vol. 101, Sep. 2008, Art. ID 113901.
[8] A. Sentenac and P. C. Chaumet, "Subdiffraction light focusing on a grating substrate," *Phys. Rev. Lett.*, vol. 101, Jul. 2008, Art. ID 013901.
[9] R. Merlin, "Radiationless electromagnetic interference: Evanescent-field lenses and perfect focusing," *Sci.*, vol. 317, pp. 927–929, Aug. 2007.
[10] A. Grbic, L. Jiang, and R. Merlin, "Near-field plates: Subdiffraction focusing with patterned surfaces," *Sci.*, vol. 320, pp. 511–513, Apr. 2008.
[11] A. Grbic, R. Merlin, E. M. Thomas, and M. F. Imani, "Near-field plates: Metamaterial surfaces/arrays for subwavelength focusing and probing," *Proc. IEEE*, vol. 99, no. 10, pp. 1806–1815, Oct. 2011.
[12] M. F. Imani and A. Grbic, "An experimental concentric near-field plate," *IEEE Trans. Microw. Theory Techn.*, vol. 58, no. 12, pp. 3982–3988, Dec. 2010.
[13] A. Grbic and R. Merlin, "Near-field focusing plates and their design," *IEEE Trans. Antennas Propag.*, vol. 56, no. 10, pp. 3159–3165, Oct. 2008.
[14] R. Gordon, "Proposal for superfocusing at visible wavelengths using radiationless interference of a plasmonic array," *Phys. Rev. Lett.*, vol. 102, May 2009, Art. ID 207402.
[15] L. Scorrano, F. Bilotti, and L. Vegni, "Design of a meta-screen for near-zone field focalization at optical frequencies," *Microw. Opt. Technol. Lett.*, vol. 51, no. 11, pp. 2718–2721, Nov. 2009.
[16] Y. Wang, A. M. H. Wong, L. Markley, A. S. Helmy, and G. V. Eleftheriades, "Plasmonic meta-screen for alleviating the tradeoffs in the near-field optics," *Opt. Exp.*, vol. 17, pp. 12351–12361, Jul. 2009.
[17] D. Banerjee, J. Lee, E. M. Dede, and H. Iizuka, "Kilohertz magnetic field focusing in a pair of metallic periodic-ladder structures," *Appl. Phys. Lett.*, vol. 99, Aug. 2011, Art. ID 093501.
[18] E. M. Dede, J. Lee, Y. Guo, L. Q. Zhou, M. Zhang, and D. Banerjee, "Kilohertz magnetic field focusing and force enhancement using a metallic loop array," *Appl. Phys. Lett.*, vol. 101, Aug. 2012, Art. ID 023506.
[19] H. Tanaka and H. Iizuka, "Kilohertz magnetic field focusing behavior of a single-defect loop array characterized by curl of the current distribution with delta function," *IEEE Antennas Wireless Propag. Lett.*, vol. 11, pp. 1088–1091, Sep. 2012.

This article has been accepted for inclusion in a future issue of this journal. Content is final as presented, with the exception of pagination.

10   IEEE TRANSACTIONS ON MICROWAVE THEORY AND TECHNIQUES

[20] L. Markley, A. M. H. Wong, Y. Wang, and G. V. Eleftheriades, "Spatially shifted beam approach to subwavelength focusing," *Phys. Rev. Lett.*, vol. 101, Sep. 2008, Art. ID 113901.

[21] L. Markley and G. V. Eleftheriades, "Two dimensional subwavelength focusing using a slotted meta-screen," *IEEE Microw. Wireless Compon. Lett.*, vol. 19, no. 3, pp. 137–139, Mar. 2009.

[22] P. M. Rossini *et al.*, "Brain-behavior relations: Transcranial magnetic stimulation: A review," *IEEE Eng. Med. Biol. Mag.*, vol. 29, no. 1, pp. 84–96, Jan.–Feb. 2010.

[23] S. Debener, M. Ullsperger, M. Siegel, and A. K. Engel, "Single-trial EEG-fMRI reveals the dynamics of cognitive function," *Trends Cognitive Sci.*, vol. 10, pp. 558–563, 2006.

[24] S. Yang *et al.*, "Circular coil array model for transcranial magnetic stimulation," *IEEE Trans. Appl. Supercond.*, vol. 20, no. 3, pp. 829–833, Jun. 2010.

[25] G. V. Eleftheriades and A. M. H. Wong, "Holography-inspired screens for sub-wavelength focusing in the near field," *IEEE Microw. Wireless Compon. Lett.*, vol. 18, no. 4, pp. 236–238, Apr. 2010.

[26] J. P. Dunsmore, "The discrete Fourier transformer," in *Handbook of Microwave Component Measurements: With Advanced VNA Techniques*. Hoboken, NJ, USA: Wiley, 2012.
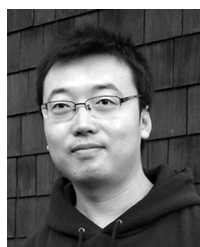
Fei Gao (S'13) received the B.Sc degree in electronic engineering from Xidian University, Xi'an, China, in 2010, and is currently working toward the Ph.D. degree at Xidian Universtiy.

He was with the National Laboratory of Science and Technology on Antennas and Microwaves (NLSTAM), Xidian University, while working toward the Master's degree. In 2011, he joined the Antenna Measurement and Antenna Design Group, NLSTAM, Xidian University, as a doctoral student. From 2011 to 2012, he was responsible for GPS antenna design with high phase center stability and ultra-wideband antenna design. Since 2012, he has been with the Applied Electromagnetics Research Group, University of California at San Diego, La Jolla, CA, USA, as a Visiting Graduate Student. His research interests include electrical amall antenna (ESA), ultra-wideband antenna, and near field technology.

Fushun Zhang received the B.Sc., M.Sc., and Ph.D. degrees in electrical engineering from Xidian University, Xi'an, China, in 1982, 1993, and 1997, respectively.

During 2002 and 2008, he performed some cooperative research as a Visiting Scholar with the City University of Hong Kong, The Central Astronomical Observatory of the Russian Academy of Sciences at Pulkovo, the National Astronomical Observatory of Japan, and the Observatoire de Paris or Observatoire de Paris-Meudon. He is an academic leader in the field of electromagnetic wave and microwave technology with Xidian University. He has been involved with about 100 research projects including the National Natural Science Foundation of China's "Genetic Algorithm (GA) in High Performance Antenna Design." He has authored or coauthored 200 technical publications. He holds a patent on " Small Log-periodic Antenna with High Gain." His current research is antenna theory, design, and measurement.

Dr. Zhang is a member of the Chinese Institute of Electronics (CIE) and the Academic Committee in the Key Laboratory of Structure Design of Electronic Equipment, Ministry of Education of China. He has been the recipient of some awards for progress in science and technology by the Ministry of Electronics Industry, China.

Ming Huang (S'11) was born in Luoyang, China, in 1986. He received the B.Sc degree in electronic and information engineering from the University of Electronic Science and Technology of China (UESTC), Chengdu, China, in 2007, and is currently working toward the Ph.D. degree at UESTC.

Since 2012, he has been with the Applied Electromagnetics Research Group, Department of Electrical and Computer Engineering, University of California at San Diego, La Jolla, CA, USA, as a Visiting doctoral student. His research interests include time-modulated antenna arrays, antenna array design and optimization, and lens antennas with variable impedance surfaces.

Dr. Huang was the recipient of the 2010 Postgraduate Young Scholar Award from the Ministry of Education of China.

Daniel F. Sievenpiper (M'94–SM'04–F'09) received the B.S. and Ph.D. degrees in electrical engineering from the University of California at Los Angeles, Los Angeles, CA, USA, in 1994 and 1999, respectively.

Since 2010, he has been a Professor with the University of California at San Diego, La Jolla, CA, USA, where his research focuses on antennas and electromagnetic structures. He was the Director of the Applied Electromagnetics Laboratory, HRL Laboratories, Malibu, CA, USA, where his research has included artificial impedance surfaces, conformal antennas, tunable and wearable antennas, and beam-steering methods. He has authored or coauthored over 50 technical publications. He holds over 60 patents.

Prof. Sievenpiper was the recipient of the URSI Issac Koga Gold Medal in 2008. In 2010, he was elected to the Antennas and Propagation Society Administrative Committee.